IEEE Access
Multidisciplinary | Rapid Review | Open Access Journal

Received June 20, 2019, accepted July 7, 2019, date of publication July 15, 2019, date of current version August 16, 2019.

Digital Object Identifier 10.1109/ACCESS.2019.2928802

FDTD Simulation of Three-Wave Scattering Process in Time-Varying Cold Plasma Sheath

YOUNGJOON LIM[1], (Student Member, IEEE), BONGKYUN SEO[2], AND SANGWOOK NAM[1], (Senior Member, IEEE)

[1]School of Electrical and Computer Engineering, Institute of New Media Communication, Seoul National University, Seoul 08826, South Korea
[2]Tech Core Design Team, SK Hynix, Icheon 17336, South Korea

Corresponding author: Sangwook Nam (snam@snu.ac.kr)

This work was supported by the Institute for Information and Communication Technology Planning and Evaluation (IITP) grant funded by the Korea Government (MSIT), Advanced and Integrated Software Development for Electromagnetic Analysis, under Grant 2019-0-00098.

ABSTRACT In this paper, a three-dimensional finite-difference time-domain (FDTD) method is developed to simulate the three-wave scattering process as a numerical experiment of the nonlinear interaction between two monochromatic plane waves in a plasma slab. This electromagnetic (EM)–plasma coupled system is governed by Maxwell's equations and the momentum equations of electron-only cold plasma. To model the system using the FDTD method, a simple and efficient periodic boundary condition is proposed and analyzed using the Floquet mode theory. The simulation result for the plasma slab with a linearly increasing electron density profile demonstrates that it is feasible to use the proposed formulations for the three-wave scattering process. Then, additional simulations are performed for the plasma slab with different electron density profiles and different incident angles of a signal wave as case studies to show the capability of the developed method for various environments.

INDEX TERMS Finite-difference time-domain (FDTD), three-wave scattering process, cold plasma Floquet mode, nonlinear phenomena.

I. INTRODUCTION

There are several interesting electromagnetic (EM)–plasma coupled phenomena, including microwave breakdown under a high-power pulse and communication blackout in re-entry vehicles [1]–[3]. In addition, there are useful applications of EM–plasma coupled systems such as microwave torches, tokamaks, and chemical vapor deposition in semiconductor processes [4]–[6]. Actual experiments for various plasma parameters are required to study EM–plasma coupled systems in depth. However, data acquisition from actual experiments for a large number of plasma parameters is inefficient in reality. An alternative is numerical experiments, in which we mathematically model a physical system and solve a mathematical problem using computer simulation. This is an extremely cost efficient method of obtaining data for a system. Among numerical techniques, the finite-difference time-domain (FDTD) method is the most widely used approach to solve EM–plasma coupled systems because it is accurate and easy to implement and parallelize [7]–[28]. In addition, the FDTD method has advantages over numerous other numerical techniques when simulation includes complex media or nonlinear phenomena [29]. Luebbers *et al.* modeled isotropic plasma as a dispersive medium with complex permittivity and solved Maxwell's equations using the recursive convolution technique [7]–[8]. Hunsberger *et al.* introduced magnetized plasma as gyrotropic media [9]. Young proposed the direct integration (DI) method and solved the equation of motion and Maxwell's equations together [10]–[11]. Samimi and Simpson proposed an explicit FDTD scheme for magnetized plasma using the Boris particle mover, which is widely used in the particle-in-cell method [22]. Cannon and Honary solved an EM–plasma coupled system by utilizing the five-moment plasma fluid model with graphical processing unit acceleration [23]. However, most of the abovementioned studies focused on time-invariant plasma and on the techniques of dealing with the dispersive and gyrotropic characteristics of plasma.

The associate editor coordinating the review of this manuscript and approving it for publication was Ladislau Matekovits.

There have been few studies on the solution of the nonlinear EM–plasma coupled problem by employing the FDTD method.

In this paper, we study the three-wave scattering process in time-varying cold plasma using the FDTD method as a numerical experiment of a nonlinear EM–plasma coupled system. The three-wave scattering process in plasma was originally proposed by Nazarenko *et al.* as a method of mitigating communication blackout in vehicles in the re-entry phase [30]. The method uses the nonlinear interaction between the signal wave from a base station and the pump wave from a vehicle. In the three-wave scattering process, an EM wave is coupled to an electrostatic (ES) wave and generates Langmuir oscillation by acting like a repeater. The three-wave scattering process has not attracted significant interest owing to its effectiveness because no linear coupling between longitudinal waves was seen in real plasma profiles during reentry [31]. However, it is worth conducting simulations for various plasma parameters because it shows single-sided mixing phenomena between monochromatic plane waves and it is physically an extremely interesting EM–plasma coupled problem, although it cannot be a solution for blackout mitigation.

The rest of the paper is organized as follows: Section II describes the simulation model for the three-wave scattering process. The physical model and the system of equations are presented. The system of equations is discretized into a set of FDTD update equations. A simple and efficient periodic boundary condition (PBC) is proposed and analyzed using the Floquet mode theory to simulate a plasma slab in the FDTD method. The numerical results and discussion are presented in section III. First, the three-wave scattering process is simulated for a linearly increasing electron density profile and compared with the analytic estimation. Then, additional case studies are performed for different electron density profiles and incident angles of a signal wave. Error analysis and future work are described in section III-C. Finally, conclusions are provided in section IV.

II. MODEL DESCRIPTION

A. PHYSICAL MODEL

The schematic for the simulation of the three-wave scattering process is presented in Fig. 1. The plasma sheath is modeled as a slab that is parallel to the xy-plane. We assume that the plasma is electron-only cold plasma and there is no magnetic bias on it. Two monochromatic plane waves are launched from each side of the slab. A signal wave ($\vec{\mathbf{k}}_{sig}$) comes from the left side of the plasma and impinges on the plasma slab at angle θ with respect to the negative z-axis. A pump wave ($\vec{\mathbf{k}}_{pump}$) comes from the right side of the plasma and impinges on the slab at angle ψ with respect to the z-axis. We assume that the frequency of the pump wave is considerably higher than that of the signal wave. In the condition described above, it is known that a scattered wave ($\vec{\mathbf{k}}_{scat}$) is generated by the nonlinear interaction between the signal wave and pump wave at the location of Langmuir oscillation. We assume that the location of Langmuir oscillation is at $z = z_{Langmuir}$, in which $f_p(z) = f_{sig}$, where f_{sig} and f_p are the frequencies of the signal wave and the plasma frequency of the sheath, respectively.

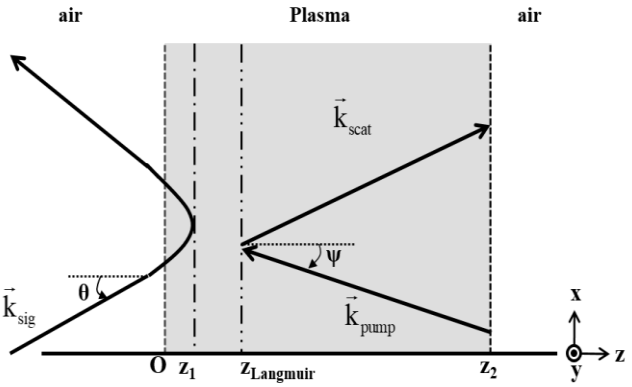

FIGURE 1. Schematic of three-wave scattering process.

The above mentioned three-wave scattering process is analogous to the Raman scattering process in nonlinear optics. When electron density increases linearly with respect to the z-axis, the scattered wave is a Stokes wave, whose frequency corresponds to the difference between the frequencies of the pump wave and signal wave. Theoretically, the signal wave can propagate until $z = z_1$, in which $f_{sig} \cdot cos\theta$ is equal to $f_p(z)$; However, when the signal wave is transverse electric to the y-axis, a part of EM wave energy is converted to an ES wave and Langmuir oscillations are excited in the plasma. The waves that are transverse magnetic (TM) to the y-axis are not considered here because it is well known that TM waves cannot be converted to ES waves.

B. FDTD UPDATE EQUATIONS

We assume that electron density N is time variant and is sum of time-invariant background electron density N_0 and time-variant perturbed electron density $\tilde{\mathbf{N}}$. Then, the behavior of electrons in plasma can be analyzed using the system of equations below, within $O(\nu/\omega)$ [32].

$$\nabla \times \vec{E} = -\mu_0 \frac{\partial \vec{H}}{\partial t} \tag{1}$$

$$\nabla \times \vec{H} - \vec{J}_L - \vec{J}_{NL} = \varepsilon_0 \frac{\partial \vec{E}}{\partial t} \tag{2}$$

$$\frac{\partial \vec{U}_L}{\partial t} + \nu \vec{U}_L = \frac{q_e}{m_e} \vec{E} \tag{3}$$

$$\frac{\partial \vec{U}_{NL}}{\partial t} = -\frac{1}{2} \nabla U_L^2 \tag{4}$$

$$\frac{\partial N}{\partial t} + \nabla \cdot (N \vec{U}) = 0 \tag{5}$$

where $\vec{\mathbf{U}}$ *and* $\vec{\mathbf{J}}$ are the velocity of electrons and electric current density, respectively. They are related according to the

equations given below.

$$\vec{J}_L = N_0 q_e \vec{U}_L \tag{6}$$
$$\vec{J}_{NL} = N_0 q_e \vec{U}_{NL} + \tilde{N} q_e \vec{U}_L \tag{7}$$

Subscripts 'L' and 'NL' denote 'linear' and 'nonlinear,' respectively. $\mathbf{q_e}$ and $\mathbf{m_e}$ are the charge quantity and mass of an electron, respectively. $\boldsymbol{\varepsilon_0}$ and $\boldsymbol{\mu_0}$ are the permittivity and permeability of free space, respectively. The system of equations consists of Maxwell's equations, two equations of motion for the linear and nonlinear velocities of electrons, and the continuity equation. The motion of electrons is transformed to a current source and coupled to Maxwell's equations using (6) and (7). Nonlinear current is due to the nonlinear response of background electrons and the nonlinear response of perturbed electron density. FDTD update equations are obtained by discretizing (1)–(5). The discretization is carried out on the conventional Yee cell. $\vec{U}_L$ and $\vec{U}_{NL}$ are collocated with $\vec{E}$ for stable coupling between Maxwell's equations and the momentum equations of the electron [22], [23]. Electron density related variables are located on all integer vertices of the Yee cell and used with appropriate averaging. The central difference scheme (CDS) is used for spatial and temporal differential operations. $\tilde{N}$ is updated in integer time. $\vec{U}$ and $\vec{J}$ are updated in half-integer time to be effectively coupled to Maxwell's equations. The discretization of (1)–(3) has been provided in numerous previous studies, and we assume that the readers are familiar with it. Thus, the discretization of (1)–(3) is not described here. We only consider the discretization of (4) and (5). Equations (4) and (5) are represented as the semi-discretized equations given below by employing the CDS.

$$\frac{\vec{U}_{NL}\Big|^{n+0.5} - \vec{U}_{NL}\Big|^{n-0.5}}{\Delta t} = -\frac{1}{2}\nabla(\vec{U}_L^n)^2 \tag{8}$$

$$\frac{\tilde{N}\Big|^{n+1} - \tilde{N}\Big|^{n}}{\Delta t} + \frac{\tilde{N}\Big|^{n+1} + \tilde{N}\Big|^{n}}{2}\nabla\cdot\vec{U}^{n+0.5} = -(N_0\nabla\cdot\vec{U}^{n+0.5} + \vec{U}^{n+0.5}\cdot\nabla N_0) \tag{9}$$

where,

$$\nabla(\vec{U}_L^n)^2 = \hat{x}\frac{1}{\Delta x}\{(U_L|^n_{i+1,j,k})^2 - (U_L|^n_{i,j,k})^2\} + \hat{y}\frac{1}{\Delta y}\{(U_L|^n_{i,j+1,k})^2 - (U_L|^n_{i,j,k})^2\} + \hat{z}\frac{1}{\Delta z}\{(U_L|^n_{i,j,k+1})^2 - (U_L|^n_{i,j,k})^2\} \tag{10}$$

$$\nabla\bullet\vec{U}^{n+0.5} = \frac{1}{\Delta x}(U_x|^{n+0.5}_{i+0.5,j,k} - U_x|^{n+0.5}_{i-0.5,j,k}) + \frac{1}{\Delta y}(U_y|^{n+0.5}_{i,j+0.5,k} - U_y|^{n+0.5}_{i,j-0.5,k}) + \frac{1}{\Delta z}(U_z|^{n+0.5}_{i,j,k+0.5} - U_z|^{n+0.5}_{i,j,k-0.5}) \tag{11}$$

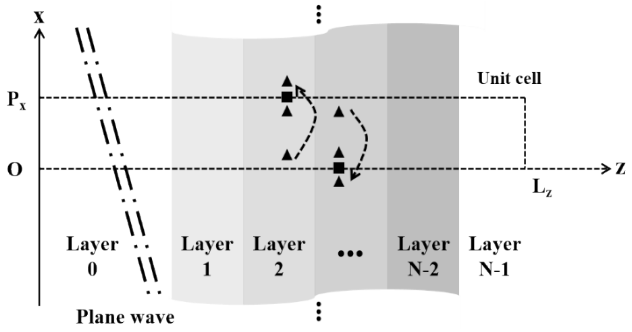

FIGURE 2. Schematic periodic boundary condition for layered media.

$$\vec{U}^{n+0.5}\cdot\nabla N_0 = \left(\frac{U_x|^{n+0.5}_{i+0.5,j,k} + U_x|^{n+0.5}_{i-0.5,j,k}}{2}\right)\times\left(\frac{N_0|_{i+1,j,k} - N_0|_{i-1,j,k}}{2\Delta x}\right) + \left(\frac{U_y|^{n+0.5}_{i,j+0.5,k} + U_y|^{n+0.5}_{i,j-0.5,k}}{2}\right)\times\left(\frac{N_0|_{i,j+1,k} - N_0|_{i,j-1,k}}{2\Delta y}\right) + \left(\frac{U_z|^{n+0.5}_{i,j,k+0.5} + U_z|^{n+0.5}_{i,j,k-0.5}}{2}\right)\times\left(\frac{N_0|_{i,j,k+1} - N_0|_{i,j,k-1}}{2\Delta z}\right) \tag{12}$$

Velocity vector $\vec{U}$ is the sum of $\vec{U}_L$ and $\vec{U}_{NL}$, and it is adequately averaged in space and time. For example,

$$U_x|^n_{i,j,k} = \frac{1}{2}\begin{pmatrix} U_{Lx}|^n_{i,j+0.5,k} + U_{Lx}|^n_{i,j-0.5,k} \\ + U_{NLx}|^n_{i,j+0.5,k} + U_{NLx}|^n_{i,j-0.5,k}\end{pmatrix} \tag{13}$$

$$U_x|^n_{position} = \frac{1}{2}\begin{pmatrix} U_{Lx}|^{n+0.5}_{position} + U_{Lx}|^{n-0.5}_{position} \\ +U_{NLx}|^{n+0.5}_{position} + U_{NLx}|^{n-0.5}_{position}\end{pmatrix} \tag{14}$$

C. BOUNDARY CONDITIONS

The plasma slab that is parallel to the xy-plane is a kind of layered media and could be treated as a periodic structure. We can assume that the periodic structure has periodicities P_x and ∞ with respect to the x-axis and y-axis, respectively, as shown in Fig. 2. When a plane wave impinges on the layered media at angle θ with respect to the z-axis, the field components at $x = P_x$ and $x = 0$ have a relationship that is expressed in the phasor domain by [33]

$$\tilde{\psi}(x = 0, y, z) = \tilde{\psi}(x = P_x, y, z)\ \exp\ (jk_xP_x) \tag{15}$$

where,

$$k_x = k_{x0} + 2m\pi/P_x \tag{16}$$
$$k_{x0} = k_0\sin\theta \tag{17}$$

k_0 is the free space wavenumber. k_{x0} is the wavenumber of the fundamental Floquet mode on the x-axis and $2m\pi/P_x$ is that of higher-order Floquet modes [34]. $\tilde{\psi}$ could be an electric or magnetic field component. m is an integer. We assume

the exp(jωt) convention. The FDTD method requires the boundary conditions to be represented in the time domain. Using the inverse Fourier transform, (15) becomes

$$\psi(x = 0, y, z, t) = \psi(x = \mathrm{P_x}, y, z, t + P_x \sin\theta/c_0) \quad (18)$$

Equation (18) shows that the PBC requires future field components. We can easily notice that the additional time delay or advance in (18) results from the fundamental Floquet mode because the wavenumbers of higher-order Floquet modes can be neglected by multiplying periodicity P_x with the argument of the exponential function in (15). When a plane wave normally impinges on the layered media, namely, $\theta = 0°$, (18) becomes

$$\psi(x = 0, y, z, t) = \psi(x = \mathrm{P_x}, y, z, t) \quad (19)$$

In this case, the field components at each boundary can be updated using those on the other side, as represented in Fig. 2.

However, when a plane wave obliquely impinges on the layered media, techniques for ignoring time delay and advance are required [29], [33]. In our simulation, two plane waves with different frequencies and incident angles should be excited. Therefore, we modified the geometry to excite two individual plane waves by utilizing the modified sin–cos method [35]. The main idea is based on the fact that the periodicity of layered media can be arbitrarily selected to make the argument of the exponential function in (15) an integer multiple of 2π. For example, let us assume there exist two plane waves, P_1 and P_2, with a pair of parameters, (θ_1, f_1, $\mathrm{P_{x1}}$) and (θ_2, f_2, $\mathrm{P_{x2}}$), respectively. θ and f are the incident angle and frequency of the plane waves, respectively. P_x is the periodicity of layered media. Subscript in parameters denotes the number of each plane wave. Then, the wavenumbers in the x-direction of the two plane waves along the x-axis are

$$\mathrm{k_{x1}} = k_{01} \sin\theta_1 + \frac{2m\pi}{P_{x1}} \quad (20)$$

$$\mathrm{k_{x2}} = k_{02} \sin\theta_2 + \frac{2n\pi}{P_{x2}} \quad (21)$$

where k_{01} and k_{02} are the free space wavenumbers of each plane wave. m and n are integers. The relationship for the field components at each boundary can be expressed in the phasor domain as

$$\tilde{\psi}_1(x = 0, y, z) = \tilde{\psi}_1(x = \mathrm{P_{x1}}, y, z) \exp(jk_{x1}\mathrm{P_{x1}}) \quad (22)$$

$$\tilde{\psi}_2(x = 0, y, z) = \tilde{\psi}_2(x = \mathrm{P_{x2}}, y, z) \exp(jk_{x2}\mathrm{P_{x2}}) \quad (23)$$

The exponential term in (22) and (23) can be neglected by selecting periodicity $\mathrm{P_x}$ such that $\mathrm{k}_{x1}P_x$ and $\mathrm{k}_{x2}P_x$ become integer multiples of 2π. This implies that time delay or advance can also be neglected for both plane waves when we excite two obliquely incident plane waves with different frequencies. For example, we can use two incident plane waves with pairs of (30°, 2 GHz, 0.3 m) and (0°, 12 GHz, 0.3 m) for simulation. It is physically evident for the scattered wave that the k_x of the source current of the wave is set by the values of k_{x1} and k_{x2}, and then, the boundary condition is automatically satisfied. With the simple modification described above, the field components at each periodic boundary can be easily updated like for the normal incidence case. It can be difficult to make $\mathrm{k}_{x1}P_x$ and $\mathrm{k}_{x2}P_x$ exact integer multiples of 2π in a practical manner. Through computer simulation, we found that a phase error of less than 3° is acceptable for the proposed method and a phase error of 2.4° leads to a difference of approximately 0.02% in results. The smaller phase error can be achieved through denser spatial sampling. This method is highly efficient because the legacy code is reusable even though computational burden increases when a large number of plane waves with extreme incident angles must be supported.

III. NUMERICAL RESULTS AND DISCUSSION

It is critical to determine appropriate grid and time intervals before performing the numerical simulations for accurate simulation results. The conventional FDTD method generally recommend using a grid interval of less than $\boldsymbol{\lambda/10}$, where $\boldsymbol{\lambda}$ denotes the wavelength of the maximum frequency in the performed simulation. When the grid interval is determined once, time interval is automatically determined by the Courant–Friedrichs–Lewy number (CFLN) [29]. The CFLN of the simulation is determined to be less than one to ensure the stability of the FDTD simulation of Maxwell's equations. The CFLN in free space is defined as

$$CFLN = \frac{c\Delta t\sqrt{N}}{\Delta x} \quad (24)$$

where $\mathbf{c}$, $\Delta\mathbf{t}$, $\mathbf{N}$, and $\Delta\mathbf{x}$ are the velocity of light in free space, time interval, dimension of simulation, and grid interval, respectively. In all numerical simulations presented in this section, the frequencies of the signal wave and the pump wave are set to 2 GHz and 12 GHz, respectively. It is well known from the three-wave scattering process theory that the scattered field is a Stokes wave and is expected to have a frequency of 10 GHz. As a result, it is reasonable to determine the maximum frequency of the simulations be 15 GHz with buffers in the frequency domain. The grid and time interval used in all numerical experiments are set to be $\boldsymbol{\Delta} = 0.002$ m in all directions with a CFLN of 0.9. The grid interval corresponds to $\boldsymbol{\lambda/10}$ of the maximum frequency determined in free-space. The limits described above only ensure the stability of the FDTD method for Maxwell's equations. The stability analysis for the entire system of equations, including the momentum equations of electrons, should be presented and applied for simulations. However, the conventional methods of checking the stability and numerical dispersion limits (e.g., complex frequency analysis and Von Neumann analysis) are not applicable for the proposed nonlinear formulation and there is no unified scheme for solving all nonlinear problems [36]. Therefore, the stability limits for the numerical experiments are determined based on a numerical convergence test. Details are described in section III-C.

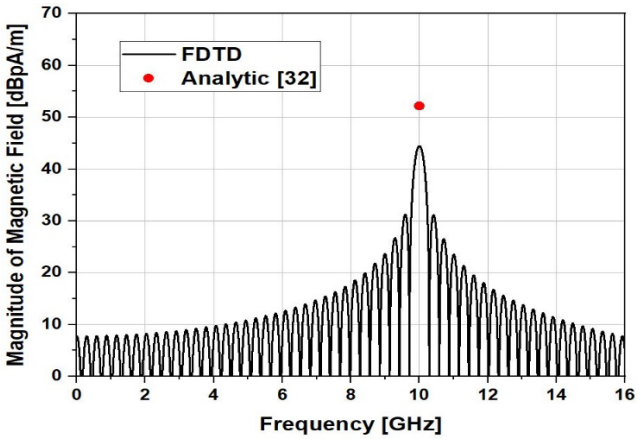

FIGURE 3. Magnitude of magnetic field of scattered wave for linearly increasing electron density profile.

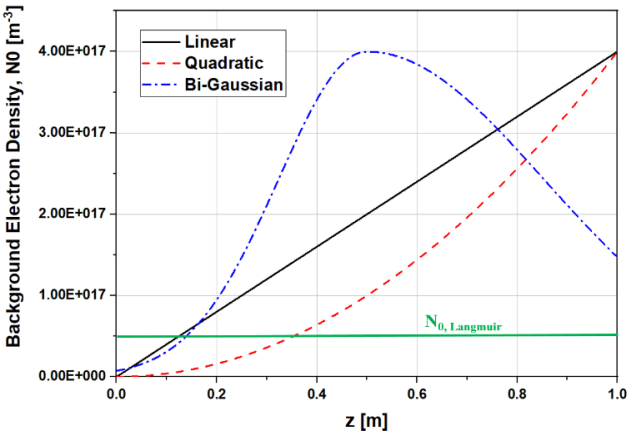

FIGURE 4. Background electron density (N_0) profiles for case study.

A. LINEARLY INCREASING ELECTRON DENSITY PROFILE

In this section, we present the FDTD simulation results of the three-wave scattering process for a linearly increasing density profile as a validation example because the analytic estimation of the three-wave scattering process for a linearly increasing electron density profile (N_{Lin}) has been extensively analyzed using complex integration [32]. The initial electron density is expressed as

$$N_{Lin}(x, y, z) = \begin{cases} N_{\max} z & (0 \le z \le z_2) \\ 0 & otherwise \end{cases} \tag{25}$$

where $\mathbf{N}_{max}$ is the maximum density of background electrons. We set $\mathbf{N}_{max}$ to be $\mathbf{1.0{\times}10^{18}m^{-3}}$. The plasma slab has a thickness of 1 m ($\mathbf{z_2 = 1}$). The signal wave and pump wave are excited using the total-field scattered-field [29] technique in the air region and vehicle region, which face each other as shown in Fig. 1, with incident angles $\boldsymbol{\theta}$ and $\boldsymbol{\psi}$, respectively. The computational domain has a size of 0.3 m, 0.004 m, and 1.2 m along the $x-$, $y-$, and z-axis, respectively. The computational domain is terminated with the proposed PBC algorithm in the x-direction, a perfect magnetic conductor in the y-direction, and with the 10-cell thickness of the convolutional perfectly matched layer (CPML) [37] in the z-direction. The reflected and transmitted plane waves are absorbed in the CPML. The interactions between the open boundaries of the plasma slab and the air are assumed to be negligible therefore the contacts between the plasma slab and the air are time invariant. The simulation result for the magnitude of the magnetic field of the scattered wave is shown in Fig. 3. The FDTD simulation result is compared with the analytic estimation given in [32]. As expected, the scattered wave has a frequency of 10 GHz and the simulation result demonstrates good agreement with the analytic estimation in terms of the frequency of the scattered field.

B. CASE STUDY: EFFECTS OF ELECTRON DENSITY PROFILES AND INCIDENT ANGLES OF SIGNAL WAVE

First, case studies are performed for different electron density profiles, i.e., Bi-Gaussian ($N_{Bi-G.}$) and quadratic (N_{Quad}) functions, on the z-axis. Background electron density profiles are expressed as

$$N_{Bi-G.}(x, y, z) = \begin{cases} N_{\max} \exp\left(-\left(\dfrac{z - z_c}{w_1}\right)^2\right) & (0 \le z \le z_c) \\ N_{\max} \exp\left(-\left(\dfrac{z - z_c}{w_2}\right)^2\right) & (z_c < z \le z_2) \\ 0 & otherwise \end{cases} \tag{26}$$

$$N_{Quad}(x, y, z) = \begin{cases} N_{\max} z^2 & (0 \le z \le z_2) \\ 0 & otherwise \end{cases} \tag{27}$$

These profiles with the location of Langmuir oscillation are depicted in Fig. 4. We set density parameters N_{max}, w_1, w_2, and z_c to be $4.0{\times}10^{17}\mathrm{m}^{-3}$, 0.25, 0.5, and 0.5, respectively. It is evident that any complex density profile along the z-axis can be solved by changing the plasma parameters. The FDTD simulation results for different electron density profiles are shown in Fig. 5, which presents the magnitude of the magnetic field of the scattered wave in the frequency domain. The strongest scattered wave occurs for the Bi-Gaussian electron density because dominant source of the scattered wave is the electron density perturbed by the signal wave and its interaction with the pump wave. It could be analytically estimated that the perturbed electron density is proportional to the slope of background electron density at the location of Langmuir oscillations; the simulation results are in good agreement with the analytic estimation [32]. The shape of the Langmuir oscillation is presented in Fig. 6 through the magnitude of the perturbed electron density. The figure shows that the magnitude of the scattered field is proportional to the magnitude of the Langmuir oscillations.

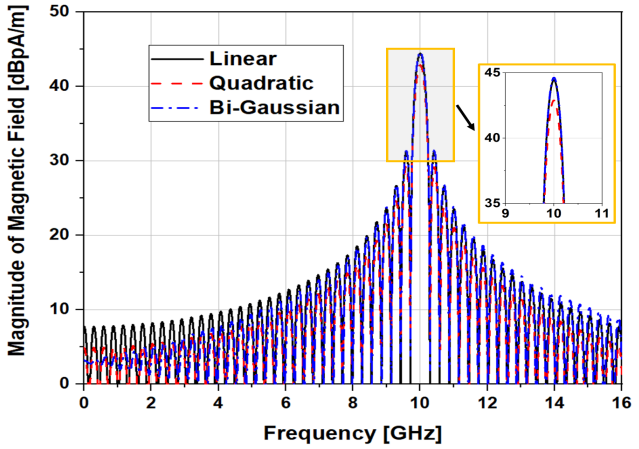

FIGURE 5. Magnitude of magnetic field of the scattered wave for different electron density profiles.

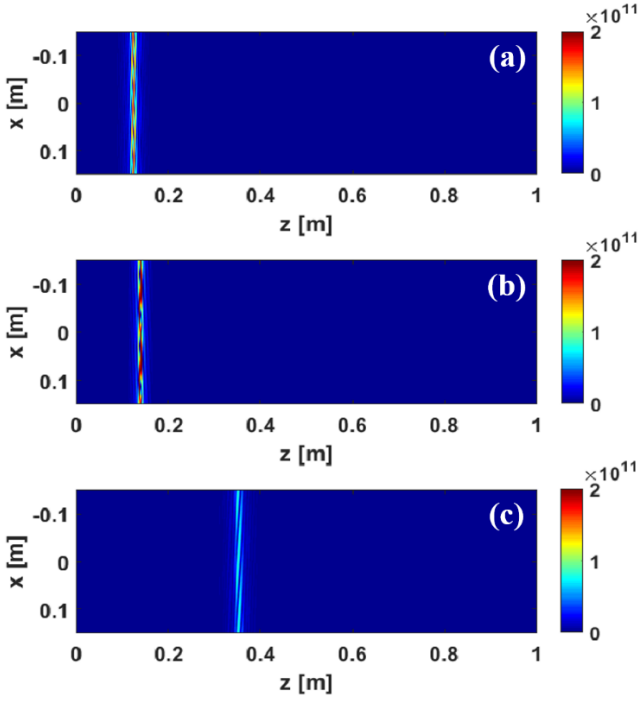

FIGURE 6. Magnitude of the perturbed electron density for different electron density profiles: (a) Linear, (b) Bi-Gaussian, and (c) Quadratic.

Second, additional simulations are conducted for different incident angles of the signal wave with the linearly increasing electron density profile shown in Fig. 4. The simulation results are presented in Fig. 7. The maximum scattered wave occurs when $\theta = 30°$ and the results agree well with those of the analytical estimation. It is also known that the optimum angle of the pump wave, i.e., ψ, is 0° as considered in our study.

C. DISCUSSION

The FDTD simulation results of the three-wave scattering process shows a certain disagreement with the theory in terms of magnitude, even though the results show good agreement

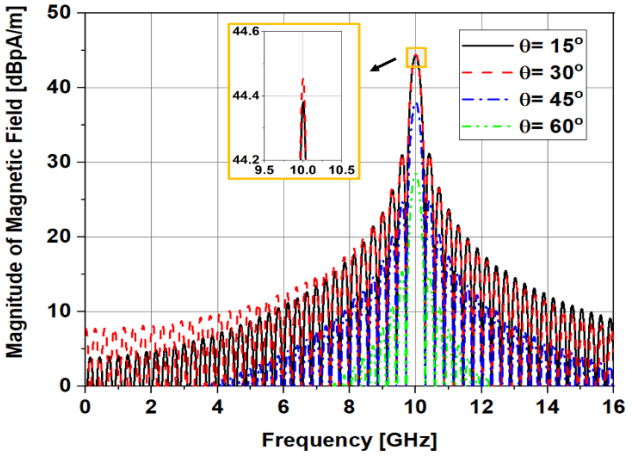

FIGURE 7. Magnitude of the magnetic field of the scattered wave for different incident angles of the signal wave.

in terms of frequency. The disagreement is expected to be due to the following reasons:

- Analytic estimation cannot include dynamically varying electron density and simultaneous interactions between waves. It only calculates the physical quantities in the steady state.
- The magnitude of the scattered wave is $10^{-6}10^{-7}$ times that of the pump wave. Small errors could lead to a large difference between analytic estimation and FDTD simulation values.

The lack of stability and dispersion analysis for the proposed algorithm is also an issue, and it should be resolved. It is well known that the stability of the DI method based FDTD algorithm can be ensured using the conventional CFLN when the following conditions are satisfied [13], [16].

- The plasma is not magnetically biased.
- The nodes for $\vec{U}(or\vec{J})$ are collocated with $\vec{E}$ and updated at the same time as $\vec{H}$.
- Only the 1st order momentum equation, i.e., the equation of motion, is considered for election.

In our method, the 0th order momentum equation, i.e., the charge conservation equation, and the equation for nonlinear velocity are considered along with Maxwell's equation. Thus, the conventional CFLN cannot be the stability criterion. Instead, we performed convergence tests for various CFLNs that were close to 1. The simulation results are presented in Fig. 8. When the CFLN is almost 1 or higher, the simulation diverged as expected. Thus, we set the CFLN to 0.9 with a margin to overcome the unexpected source of instability factors.

The momentum equations for the fluid model used in this study are only the 0th and 1st order equations with scattering frequency between electrons and neutrals. However, the simulation model could be extended by utilizing a higher-order momentum fluid model and various scattering parameters. Electron energy and temperature could be calculated by including the 2nd order momentum equation of electrons. The

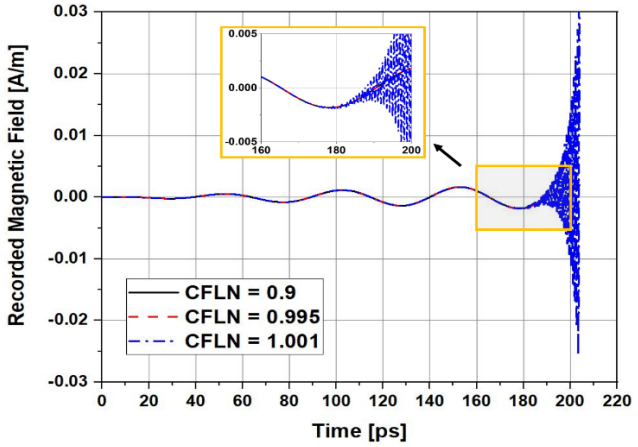

FIGURE 8. Time record of magnetic field at the five Yee-cells from the source point for different CFLNs.

generation and attachment processes of electrons could be considered by including additional scattering parameters.

These aspects remain as future works.

IV. CONCLUSION

An FDTD simulation method for the three-wave scattering process is presented as a numerical experiment of the nonlinear interaction between waves in time-varying cold plasma. The simulation result for linearly increasing electron density shows good agreement with analytic estimation in terms of frequency responses. Case studies show that the three-wave scattering process is easily simulated through the FDTD simulation for various electron density profiles and incident angles of the signal wave, even though there is no analytic solution of the scattering process. The incident angle of the signal wave for the maximum Stokes wave is in good agreement with the analytic estimation. As we used an extremely simple model of plasma, a more extended model should be incorporated to be used in practical problems by employing various collisional processes and higher-order momentum equations. Moreover, additional studies will be constructed in the future for numerical stability and dispersion limits in detail.

REFERENCES

[1] S. Yan, A. D. Greenwood, and J.-M. Jin, "Simulation of high-power microwave air breakdown modeled by a coupled Maxwell–Euler system with a non-Maxwellian EEDF," *IEEE Trans. Antennas Propag.*, vol. 66, no. 4, pp. 1882–1893, Apr. 2018.

[2] J. P. Rybak and R. J. Churchill, "Progress in reentry communications," *IEEE Trans. Aerosp. Electron. Syst.*, vol. AES-7, no. 5, pp. 879–894, Sep. 1971.

[3] J. P. Rybak, "Causes, effects and diagnostic measurements of the reentry plasma sheath," Air Force Cambridge Res. Lab., El Segundo, CA, USA, Tech. Rep. AFCRL-70-0707, 1970.

[4] K. Kim, J. M. Park, S. Choi, J. Kim, and S. H. Hong, "Comparative study of two- and three-dimensional modeling on arc discharge phenomena inside a thermal plasma torch with hollow electrodes," *Phys. Plasmas*, vol. 15, no. 8, Feb. 2008, Art. no. 023501.

[5] F. F. Chen, *Introduction to Plasma Physics and Controlled Fusion*, 2nd ed. New York, NY, USA: Plenum Press, 1984.

[6] W. N. G. Hitchon, *Plasma Processing for Semiconductor Fabrication*, 1st ed. Cambridge, U.K.: Cambridge Univ. Press, 1999.

[7] R. J. Luebbers, F. Hunsberger, and K. S. Kunz, "A frequency-dependent finite-difference time-domain formulation for transient propagation in plasma," *IEEE Trans. Antennas Propag.*, vol. 39, no. 1, pp. 29–34, Jan. 1991.

[8] R. J. Luebbers and F. Hunsberger, "FDTD for Nth-order dispersive media," *IEEE Trans. Antennas Propag.*, vol. 40, no. 11, pp. 1297–1301, Nov. 1992.

[9] F. Hunsberger, R. Luebbers, and K. Kunz, "Finite-difference time-domain analysis of gyrotropic media. I. Magnetized plasma," *IEEE Trans. Antennas Propag.*, vol. 40, no. 12, pp. 1489–1495, Dec. 1992.

[10] J. L. Young, "A full finite difference time domain implementation for radio wave propagation in a plasma," *Radio Sci.*, vol. 29, no. 6, pp. 1513–1522, Nov/Dec. 1994.

[11] J. L. Young, "Propagation in linear dispersive media: Finite difference time-domain methodologies," *IEEE Trans. Antennas Propag.*, vol. 43, no. 4, pp. 422–426, Apr. 1995.

[12] D. F. Kelley and R. J. Luebbers, "Piecewise linear recursive convolution for dispersive media using FDTD," *IEEE Trans. Antennas Propag.*, vol. 44, no. 6, pp. 792–797, Jun. 1996.

[13] S. A. Cummer, "An analysis of new and existing FDTD methods for isotropic cold plasma and a method for improving their accuracy," *IEEE Trans. Antennas Propag.*, vol. 45, no. 3, pp. 392–400, Mar. 1997.

[14] J. H. Lee and D. K. Kalluri, "Three-dimensional FDTD simulation of electromagnetic wave transformation in a dynamic inhomogeneous magnetized plasma," *IEEE Trans. Antennas Propag.*, vol. 47, no. 7, pp. 1146–1151, Jul. 1999.

[15] J. L. Young and R. O. Nelson, "A summary and systematic analysis of FDTD algorithms for linearly dispersive media," *IEEE Antennas Propag. Mag.*, vol. 43, no. 1, pp. 61–126, Feb. 2001.

[16] W. Hu and A. S. Cummer, "An FDTD model for low and high altitude lightning-generated EM fields," *IEEE Trans. Antennas Propag.*, vol. 54, no. 5, pp. 1513–1522, May 2006.

[17] G. Cerri, F. Moglie, R. Montesi, P. Russo, and E. Vecchioni, "FDTD solution of the Maxwell–Boltzmann system for electromagnetic wave propagation in a plasma," *IEEE Trans. Antennas Propag.*, vol. 56, no. 8, pp. 2584–2588, Aug. 2008.

[18] C. Tsironis, T. Samaras, and L. Vlahos, "Scattered-field FDTD algorithm for hot anisotropic plasma with application to EC heating," *IEEE Trans. Antennas Propag.*, vol. 56, no. 9, pp. 2988–2994, Sep. 2008.

[19] Y. Yu, J. Niu, and J. J. Simpson, "A 3-D global earth-ionosphere FDTD model including an anisotropic magnetized plasma ionosphere," *IEEE Trans. Antennas Propag.*, vol. 60, no. 7, pp. 3246–3256, Jul. 2012.

[20] A. A. Al-Jabr, M. A. Alsunaidi, T. Ng, and B. S. Ooi, "A simple FDTD algorithm for simulating EM-wave propagation in general dispersive anisotropic material," *IEEE Trans. Antennas Propag.*, vol. 61, no. 3, pp. 1321–1326, Mar. 2013.

[21] M. Surkova, W. Tierens, I. Pavlenko, D. V. Eester, G. V. Oost, and D. D. Zutter, "3-D discrete dispersion relation, numerical stability, and accuracy of the hybrid FDTD model for cold magnetized Toroidal plasma," *IEEE Trans. Antennas Propag.*, vol. 62, no. 12, pp. 6307–6316, Dec. 2014.

[22] A. Samimi and J. J. Simpson, "An efficient 3-D FDTD model of electromagnetic wave propagation in magnetized plasma," *IEEE Trans. Antennas Propag.*, vol. 63, no. 1, pp. 269–279, Jan. 2015.

[23] P. D. Cannon and F. Honary, "A GPU-accelerated finite-difference time-domain scheme for electromagnetic wave interaction with plasma," *IEEE Trans. Antennas Propag.*, vol. 63, no. 7, pp. 3042–3054, Jul. 2015.

[24] W. Chen, L. Guo, J. Li, and S. Liu, "Research on the FDTD method of electromagnetic wave scattering characteristics in time-varying and spatially nonuniform plasma sheath," *IEEE Trans. Plasma Sci.*, vol. 44, no. 12, pp. 3235–3242, Dec. 2016.

[25] Y. Zhang, Y. Liu, and X. Li, "A 2-D FDTD model for analysis of plane wave propagation through the reentry plasma sheath," *IEEE Trans. Antennas Propag.*, vol. 65, no. 11, pp. 5940–5948, Nov. 2017.

[26] X.-K. Wei, W. Shao, and X.-H. Wang, "Hybrid sub-gridded time-domain method for ground penetrating radar simulations including dispersive materials," *IEEE Access*, vol. 6, pp. 15777–15786, 2018.

[27] W. Meng and L. Qian, "MedFDTD: A parallel and open-source cross-platform framework for bioelectromagnetics field simulation," *IEEE Access*, vol. 6, pp. 12940–12944, 2018.

[28] L. Zhang, L. Zhang, B. Wang, S. Liu, and C. Papavassilious, "Hybrid prediction method for the electromagnetic interference characteristics of printed cicuit boards based on the equivalent dipole model and the finite-difference time domain method," *IEEE Access*, vol. 6, pp. 6520–6529, 2017.

[29] A. Taflove and S. C. Hagness, *Computational Electrodynamics*, 2nd ed. Norwood, MA, USA: Artech House, 2005.
[30] S. V. Nazarenko, A. C. Newell, and V. E. Zakharov, "Communication through plasma sheaths via Raman (three-wave) scattering process," *Phys. Plasma*, vol. 1, no. 9, pp. 2827–2834, Sep. 1994.
[31] R. A. Hartunian, G. E. Stewart, S. D. Fergason, T. J. Curtiss, and R. W. Seibold, "Causes and mitigation of radio frequency (RF) blackout during reentry of reusable launch vehicles," Volpe Nat. Transp. Syst. Center, U.S. Dept. Transp., Cambridge, MA, USA, Aerosp. Rep. ATR-2007(5309)-1, Jan. 2007.
[32] A. O. Korotkevich, A. C. Newell, and V. E. Zakharov, "Communication through plasma sheath," *J. Appl. Phys.*, vol. 102, no. 8, Oct. 2007, Art. no. 083305.
[33] F. Yang, J. Chen, R. Qiang, and A. Z. Elsherbeni, "A simple and efficient FDTD/PBC algorithm for scattering analysis of periodic structures," *Radio Sci.*, vol. 42, no. 4, pp. 1–9, Aug. 2007.
[34] A. K. Bhattacharyya, *Phased Array Antennas: Floquet Analysis, Synthesis, Bfns, And Active Array Systems*. Hoboken, NJ, USA: Wiley, 2006.
[35] Y. Lim, B. Seo, and S. Nam, "The least common multiple sin-cos method for FDTD simulation of stratified media at oblique incidences with different frequencies," in *Proc. IEEE AP-S Symp. Antennas Propag. URSI CNS/USNC Joint Meeting (AP-S/URSI)*, Jul. 2018.
[36] J.-M. Jin and S. Yan, "Multiphysics modeling in electromagnetics: Technical challenges and potential solutions," *IEEE Antennas Propag. Mag.*, vol. 61, no. 2, pp. 14–26, Apr. 2019.
[37] J. A. Roden and S. D. Gedney, "Convolutional PML (CPML): An efficient FDTD implementation of the CFS-PML for arbitrary media," *Microw. Opt. Technol. Lett.*, vol. 27, no. 5, pp. 334–339, 2000.

YOUNGJOON LIM (S'12) received the B.S. degree in semi-conductor science from Dongguk University, Seoul, South Korea, in 2012. He is currently pursuing the Ph.D. degree. His main interest includes finite-difference time-domain method and its applications to plasma physics analysis.

BONGKYUN SEO received the B.S. degree in electrical engineering from Sungkyunkwan University, Suwon, South Korea, in 2015, and the M.S. degree in electrical and computer engineering from Seoul National University, Seoul, South Korea, in 2019. Since 2019, he has been with SK Hynix, Icheon, South Korea. His main interest includes analysis/design of RF systems.

SANGWOOK NAM (S'87–M'88–SM'11) received the B.S. degree from Seoul National University, Seoul, South Korea, in 1981, the M.S. degree from the Korea Advanced Institute of Science and Technology, Seoul, in 1983, and the Ph.D. degree from The Texas at Austin, Austin, TX, USA, in 1989, all in electrical engineering. From 1983 to 1986, he was a Researcher with the Gold Star Central Research Laboratory, Seoul. Since 1990, he has been a Professor with the School of Electrical Engineering and Computer Science, Seoul National University. His current research interests include the analysis/design of electromagnetic structures, antennas, and microwave active/passive circuit.